Experimental and theoretical study of the optical properties of FeAl alloy

1997 J. Phys.: Condens. Matter 9 11227

(http://iopscience.iop.org/0953-8984/9/50/023)

J. Phys.: Condens. Matter **9** (1997) 11227–11238. Printed in the UK PII: S0953-8984(97)86485-5

Experimental and theoretical study of the optical properties of FeAl alloy

V N Antonov†, O V Krasovska†, E E Krasovskii†, Yu V Kudryavtsev†, V V Nemoshkalenko†, B Yu Yavorsky†, Y P Lee‡ and K W Kim‡

† Institute of Metal Physics, National Academy of Sciences of Ukraine, 36 Vernadsky Street, 252680, Kiev-142, Ukraine

‡ Department of Physics, Sunmoon University, 100 Galsan-Ri, Tangjeong-Myeon, Asan, Choongnam, 336-840, Korea

Received 24 July 1997, in final form 17 October 1997

Abstract. Optical properties of ordered and disordered FeAl alloy films have been measured in the 0.5–5.0 eV energy range. The influence of the order–disorder structural transition on the optical properties of FeAl compounds has been studied. Experimental results for ordered FeAl are compared with the results of *ab initio* semi-relativistic extended linear augmented-plane-wave calculations, and explained in terms of the electronic energy band structures.

1. Introduction

Monoaluminides of the 3d transition metals (Fe, Co, and Ni) exist over a wide concentration range. Their high corrosion and oxidation resistance, and interesting magnetic properties have led to them being used in a number of applications, e.g. as high-temperature structural materials and soft magnetic materials [1]. The equiatomic alloy FeAl (β-phase) crystallizes in a CsCl-type (B2) crystal structure [2]. Because of a significant charge transfer from Al to Fe—in other words, a significant ionic contribution to the metal bonding—this alloy is very stable over a large temperature range [3, 4].

In contrast to the case for the ordered state of FeAl alloy, in the disordered one, Fe and Al atoms randomly occupy the sites of a bcc lattice. This change in the symmetry and the basis of the unit cell itself should lead to drastic changes in the electronic energy band structure. Moreover, an increase in the lattice parameter of the disordered state is often connected with an increase in the atomic radius of Al, caused by a charge transfer in the opposite direction—from Fe to Al [5]. Therefore it could be expected that the order–disorder transformation in nearly equiatomic FeAl alloys will lead to the changes in the optical properties. In the present work we are the first to study this process experimentally.

An unambiguous interpretation of the optical spectra requires *ab initio* calculations of the electronic structures of the substance. The aim of the theoretical analysis is to assign the experimentally observed spectral features to specific electronic excitations in the Brillouin zone (BZ). Most of the recent *ab initio* calculations are based on the density-functional theory (DFT) [6]. For the calculations of the ground-state properties of an electronic system, the most important approximation within the DFT is the local-density approximation (LDA) [7]. Within the LDA it is not possible to exclude the electron self-interaction [8]; however, in cases where excited states are involved, e.g. in the calculation of

0953-8984/97/5011227+12$19.50

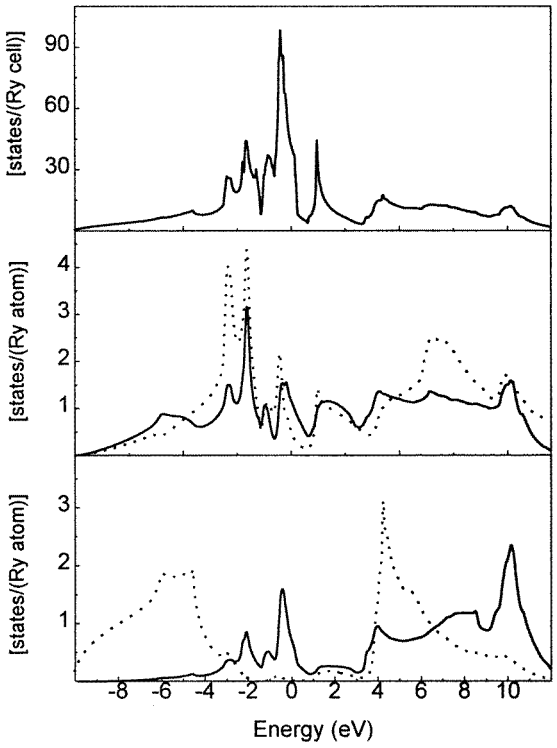

Figure 1. The upper panel shows the total density of states of FeAl. In the central panel, the partial p-projected DOS of Fe is given by the solid line, while the p-projected DOS of Al is given by the dotted line. The lower panel shows the s- and d-projected DOS of Al as dotted and solid lines respectively.

the dielectric function, the one-electron approximation is itself questionable. Nevertheless, the resulting eigenvalues and eigenvectors are in practice associated with single-particle excitation energies and wavefunctions. For conductors it is often possible to obtain good results for the optical properties within the LDA without taking into account many-body effects.

2. Electronic structures of the ordered FeAl alloy

2.1. Computational details

To solve the Schrödinger equation we have used the self-consistent semi-relativistic extended linear augmented-plane-wave method. The formalism of the extended linear augmented-plane-wave (ELAPW) method has been described in reference [9]. In the present work we do not take into account the deviations of the one-electron crystal potential from the muffin-tin form. With the muffin-tin radii $S_{\mathrm{Fe}} = 1.32$ Å and $S_{\mathrm{Al}} = 1.19$ Å, the touching spheres comprise ∼70% of the unit cell. The lattice constant of the annealed bulk FeAl sample on which the measurements were made was determined by x-ray diffraction to be $a = 2.908$ Å, and this value was used in the band-structure calculation. The exchange–correlation potential was constructed following Hedin and Lundqvist [10]. The electron

wavefunction was a linear combination of 341 energy-independent augmented plane waves (APWs) and 26 localized functions of angular momenta up to $l_{max} = 2$ for Fe and up to $l_{max} = 1$ for Al. The plane-wave cut-off was $|\boldsymbol{G}_{max}|r = 11$, with $\boldsymbol{G}_{max}$ being the longest reciprocal-lattice vector used in the APW set, and r the radius of the smallest muffin-tin sphere.

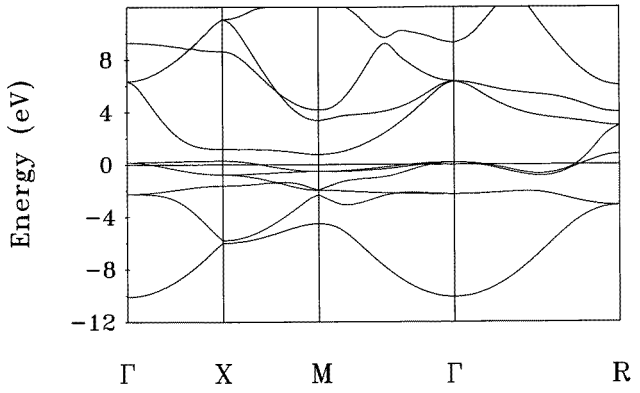

Figure 2. The energy band structure of FeAl.

The core states were included in the self-consistent procedure and were treated fully relativistically via an atomic-like calculation. In constructing the density-of-states (DOS) functions and optical spectra, we integrated over the irreducible BZ (the IBZ = 1/48 of the BZ) using the tetrahedron method [11] with a mesh of 455 $\boldsymbol{k}$-points (1728 tetrahedra) in the IBZ. The Fermi surface (FS) and the surfaces of constant energy difference were constructed by linear interpolation of the function $E_\lambda(k)$ using the tetrahedron method.

2.2. Results and discussion

The electronic structure of FeAl has been extensively studied experimentally by soft-x-ray emission spectroscopy [3, 12–16] and theoretically with the APW [17], KKR [3], hybridized nearly-free-electron tight-binding (H-NFE-TB) [18], LMTO [4, 19, 20], and FLAPW [21, 22] methods.

Calculated total and l-projected partial DOS curves are shown in figure 1. The energy zero is taken at the Fermi level. The present energy band structure and all of the features of the DOS agree perfectly with other self-consistent results [3, 4, 18–21]. The region close to the Fermi level in FeAl is determined by Fe d states. The specific-heat measurements [23] give the DOS at the Fermi level as $N(E_F) = 31.3$ states Ryd^{-1}/cell. Our value of 41.9 is much larger than the experimentally observed one. Eibler and Neckel's [18] value obtained by the H-NFE-TB method was 42.9; Koenig and Khan's [4] LMTO value was 40.1. We have also performed a spin-polarized LMTO band-structure calculation. It gives $N(E_F) = 34$ states Ryd^{-1}/cell (29.1 for minority spins and 4.9 for majority spins). This result is in agreement with the spin-polarized LMTO calculation of Sundararajan *et al* [20] and it is in better agreement with the experimental one than all of the spin-integrated calculations; however, there is no experimental evidence of the existence of local magnetic moments in this compound.

The Fermi surface of FeAl has been studied theoretically on the basis of the self-consistent band-structure calculations made by the LMTO [4] and FLAPW [22] methods.

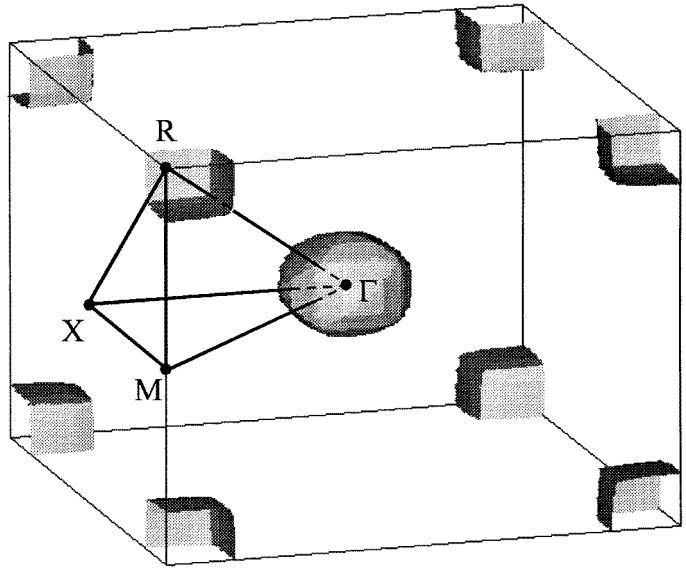

(a)

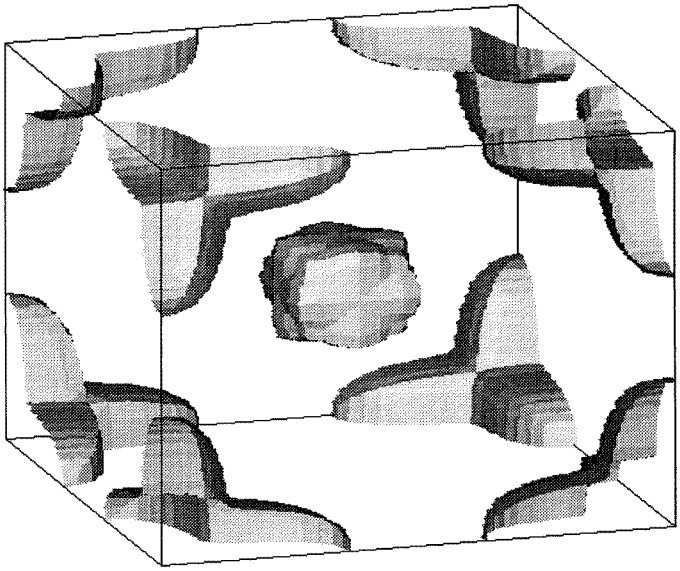

(b)

Figure 3. The Fermi surface for FeAl: sheets for the (a) fourth, (b) fifth, and (c) sixth bands.

Only high-symmetry cross-sections of the FS have been presented. In the present work we have constructed a three-dimensional model of the FS of FeAl.

Three energy bands, $\lambda = 4, 5, 6$, intersect the Fermi level (see figure 2), which leads to the FS consisting of six sheets. 3D computer-generated projections of all of the sheets are shown in figure 3. The fourth band yields two hole pockets. The nearly spherical one is located around the Γ point, and the other one is situated at R and looks like a cube with

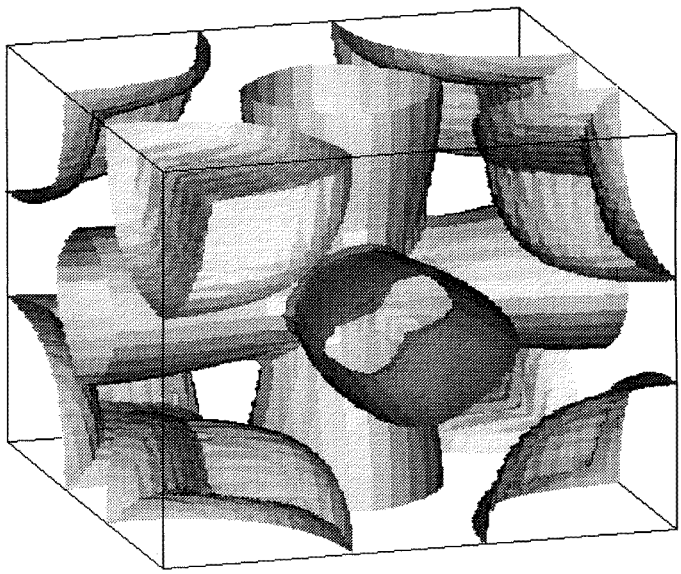

(c)

Figure 3. (Continued)

rounded edges. Each of the two pockets is enclosed in another closed hole sheet, the larger sheets being due to the fifth energy band. The shape of the fifth band pocket at Γ is far from spherical, and the sheet at R is stretched out along the R–M direction. The sixth band gives rise to two more sheets. The first one is a closed hole surface centred at R, which embraces the two pockets at this point discussed above, and the second one is the multiply connected set of hole tubes parallel to the Γ–X line.

Our model agrees well with the former theoretical results. To our knowledge there have not been reported any measurements of the de Haas–van Alphen oscillations or other related effects for this compound.

The lineshape of the Al Kβ and Fe K$\beta_{2,5}$ emission spectra of FeAl is determined by the shape of the Al p and Fe p DOS curves respectively. The energy location of the main features of our theoretical spectra is in agreement with Al Kβ measurements [12] and Fe K$\beta_{2,5}$ measurements [3, 13, 14]. The Fe L_3 emission spectrum is determined by the Fe d-like valence states. Our Fe d-projected DOS is in very good agreement with the Fe L_3 emission experiment [15].

The Al $L_{2,3}$ emission spectrum [16] is determined by the energy distribution of both s and d character in the sphere of Al. We attribute the shoulder in the high-energy part of the Al $L_{2,3}$ spectrum to transitions from the valence Fe d states which have a considerable admixture of Al d character. The main broad peak of the spectrum is due to the contribution from the Al s character.

3. Optical spectra

3.1. Theoretical results

The standard theoretical approach in analysing the response of a solid to an external electric field is through a response function. In the case of the optical properties it is

the dielectric function (DF). In the present work we derive the DF from accurate band-structure calculations. This allows us to assign the spectral features to specific excitations in the BZ.

The frequency-dependent DF, $\varepsilon(\omega) = \varepsilon_1(\omega) + \mathrm{i}\varepsilon_2(\omega)$, is calculated within the self-consistent-field one-particle approach of Ehrenreich and Cohen [24]. The interband contribution to the imaginary part of the dielectric function is given as

$$\varepsilon_2(\omega) = \frac{8\pi^2 e^2}{m^2\omega^2} \sum_i^{occ} \sum_f^{unocc} \int_{BZ} |\boldsymbol{e}\cdot\boldsymbol{P}_{if}|^2 \delta(E_f^{\boldsymbol{k}} - E_i^{\boldsymbol{k}} - \hbar\omega)\, \frac{\mathrm{d}^3\boldsymbol{k}}{(2\pi)^3} \tag{1}$$

where $\boldsymbol{e}$ is the polarization vector of the electric field, m is the mass of the electron, $\boldsymbol{k}$ is a Bloch vector in the IBZ, and E_i and E_f are band energies of the initial and final states. The momentum matrix elements, $\boldsymbol{P}_{if} = \langle\Psi_{\boldsymbol{k}f}| - \mathrm{i}\boldsymbol{\nabla}|\Psi_{\boldsymbol{k}i}\rangle$, were computed as integrals over the unit cell using the formalism described elsewhere [25]. 50 energy bands were considered, of which bands 4 to 6 are not completely filled. Because the number of the bands was finite, the values of $\varepsilon_2(\omega)$ are underestimated for $\hbar\omega > 70$ eV. In the energy interval up to $\hbar\omega = 55$ eV, the contribution to the f-sum rule

$$\int_0^\infty \varepsilon_2(\omega)\omega\, \mathrm{d}\omega = \frac{2\pi^2 e^2}{m} N_{val}$$

amounts to ∼73%. The free-electron Drude contribution to ε_2 is equal to zero in the ideal-crystal approach. The interband contribution to the spectrum of the real part of the DF, $\varepsilon_1(\omega)$, was calculated by Kramers–Kronig analysis. The plasma frequency $\omega_p = 5.8$ eV which enters into the Drude-like intraband contribution to $\varepsilon_1(\omega)$

$$\varepsilon_1^{intra}(\omega) = 1 - \frac{\omega_p^2}{\omega^2} \tag{2}$$

was calculated as an integral over the Fermi surface using the tetrahedron method [11].

The optical conductivity, σ, is connected to the DF by

$$\sigma(\omega) = \frac{\omega}{4\pi}\varepsilon_2(\omega). \tag{3}$$

In figure 4 the *ab initio* optical conductivity spectrum, σ, is presented. The overall shape of the σ-spectrum is in agreement with previous optical calculations [4, 18, 19] and measurements [26] for ordered bulk FeAl. To examine the origin of the main peaks we study the band-by-band decomposition of the spectrum. The results for the six valence bands are shown in figure 4 and in table 1.

Table 1. The positions (in eV) of the main structures in the experimental and theoretical optical conductivity spectra of FeAl alloy.

Peak	Disordered film	Ordered film	Polished bulk	Annealed bulk	Theory	Transition
A	0.9	0.7	0.7	0.7	0.2	$4, 5 \rightarrow 6$
B	1.9	1.6	1.9	1.6	1.4, 1.7	$6 \rightarrow 7$, $5 \rightarrow 7$
C	2.5	2.6	2.7	2.9	2.4, 2.9	$4 \rightarrow 7$, $3 \rightarrow 7$
D	3.2, 3.7	4.2	3.1, 3.6	4.2	5.0	$2 \rightarrow 7$

There have been several attempts to explain the main features of the optical spectra in terms of the band structure of FeAl along the high-symmetry lines and planes [26, 19]. According to equation (1), the contribution to ε_2 at a given energy from a pair of bands

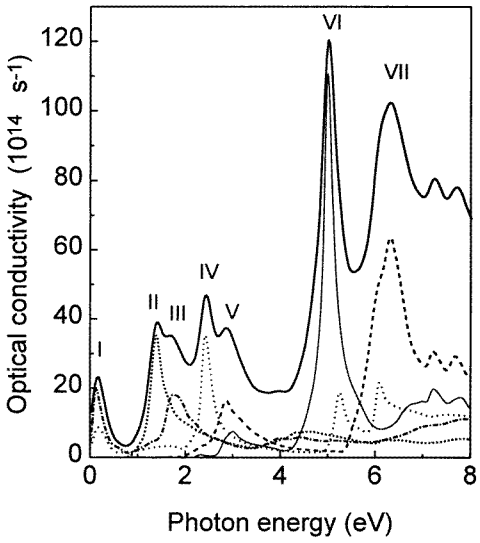

Figure 4. The calculated optical conductivity spectrum (solid line) of FeAl and the initial band-resolved contributions to it. The contributions from the bands 2, 3, 4, 5, and 6 are shown by thin solid, dashed, dotted, chain, and short-dashed lines, respectively.

is an integral over a constant-energy-difference surface in the k-space. In the metallic compounds such surfaces usually extend over large spaces in the interior of the BZ. As an example, we show in figures 5(a) and 5(b) two surfaces which are responsible for the peaks in the theoretical ε_2-spectrum at $\hbar\omega = 1.4$ eV and 5 eV respectively. It can be seen that both surfaces have very complicated shape; it is evident that the band structure along the lines and the cross-sections of the BZ does not provide the information necessary to determine the regions in k-space responsible for the optical excitations. Our spin-polarized LMTO calculation gives practically the same results. The only difference is a slight splitting ($\sim$0.2 eV) of the strong peak at 5 eV.

3.2. Experimental procedures

The equiatomic FeAl alloy was prepared by melting Fe and Al pieces of 99.99% purity in an arc furnace with a water-cooled copper hearth. In order to obtain volume homogeneity the ingot was remelted twice and then annealed at 1000 K for 6 h. One half of this ingot was used for the thin-film preparation, and the other half for structural and phase analyses, and investigation of the optical properties of the bulk FeAl alloy. For this purpose a $15 \times 10 \times 2.5$ mm sample was cut from the ingot using the spark erosion technique and then polished mechanically with diamond powders. The final stage of polishing was carried out by using Cr_2O_3 powder. To remove the surface contamination introduced by the mechanical treatment, the sample was annealed in high-vacuum conditions at 700 K for 6 h. The optical properties of bulk FeAl alloy were studied on as-polished and annealed samples.

It is known that the ordered β-phase in FeAl alloys is very stable, and that its formation cannot be completely suppressed in bulk samples by high-temperature quenching [27]. Therefore, to obtain the disordered state, vapour quenching deposition was employed, where the chaotic gas phase is condensed onto a glass substrate cooled by liquid nitrogen. The substrate temperature during the deposition was about 150 K.

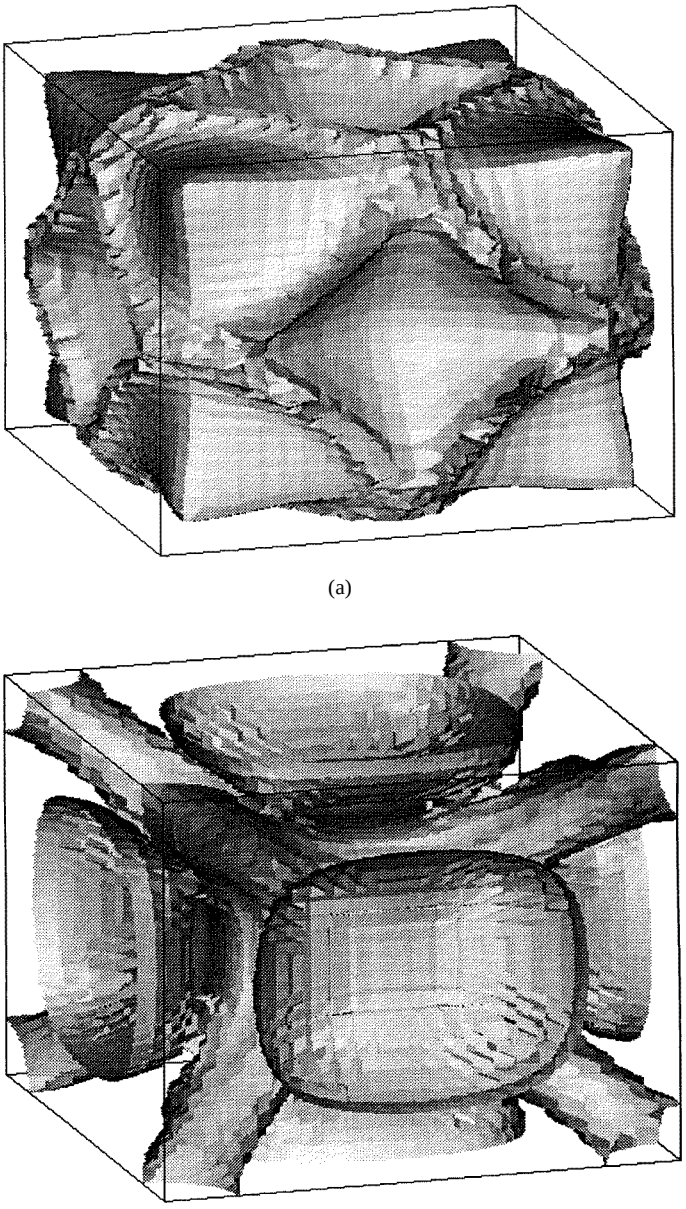

(a)

(b)

Figure 5. Constant-energy-difference surfaces, responsible for the peaks at (a) 1.4 eV and (b) 5.0 eV in the conductivity spectrum of FeAl.

For thin-film preparation, the homogeneous FeAl alloy ingot was crushed into powder consisting of particles 80–100 μm in diameter. FeAl alloy films with a total thickness of 150 nm have been prepared by means of the flash evaporation technique onto glass substrates in a high vacuum of 5×10^{-5} Pa, and the deposition rate was about 2 nm per second (such a high deposition rate keeps the volume contamination and oxidation low). An equilibrium ordered state in the FeAl alloy films was obtained by deposition onto heated

substrates, up to 680 K.

The structural analyses of the films were carried out by using transmission electron microscopy (TEM) on FeAl film samples of 60–100 nm thickness, obtained in similar conditions, deposited onto fresh chips of the monocrystalline NaCl. The x-ray fluorescence analyses for the atomic composition of the films revealed 52 at.% of Fe and 48 at.% of Al.

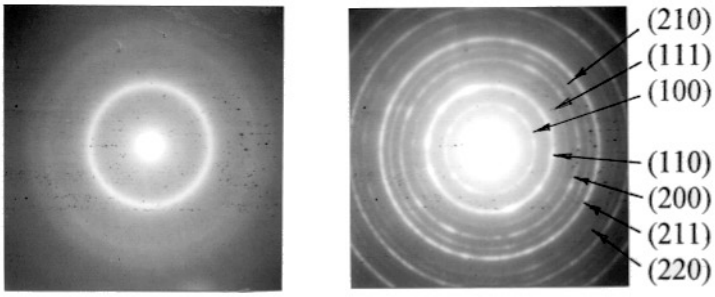

Figure 6. Transmission electron diffraction patterns of $Fe_{0.52}Al_{0.48}$ alloy films deposited onto substrates at (a) 150 K and (b) 680 K.

According to the results of the TEM study (see figure 6), the film deposition onto the glass substrates at 680 K leads to the formation of the ordered alloy structure in the $Fe_{0.52}Al_{0.48}$ films with a mean grain size of about 30 nm. A series of superstructure rings, which are attributed to the reflections from (100), (111), and (210) atomic planes, are clearly seen. This result shows that a stable phase of the superlattice, expected from the equilibrium phase diagram for the bulk FeAl system, is formed under our deposition conditions, even though the degree of long-range order (η) cannot be estimated quantitatively. A decrease in the substrate temperature to 150 K leads to the formation of considerably disordered ($\eta \sim 0$) polycrystalline films (a few smeared diffraction rings are seen) with mean grain sizes of 10–15 nm.

The optical properties (the real-n and imaginary-k parts of the complex refractive index) of the polycrystalline $Fe_{0.52}Al_{0.48}$ alloy samples were measured at room temperature in the spectral range of 250–2500 nm (5.0–0.5 eV) at a fixed incidence angle of 73° by the polarimetric Beattie technique [28]. n and k are connected to the DF by

$$\varepsilon_1 = n^2 - k^2 \qquad \varepsilon_2 = 2nk. \tag{4}$$

3.3. Discussion

The experimental optical conductivity spectra, $\sigma(\omega)$, for the ordered and disordered $Fe_{0.52}Al_{0.48}$ films and for polished bulk samples with and without annealing are shown in figure 7 for the photon energy range from 0.5 to 5 eV. Each of the spectra in this energy region has four main features, namely, a maximum below 1 eV, a broad peak between 1.5 and 2 eV, structure in the region of 2.5–3 eV, and a broad maximum above 3 eV. In figure 7 these features have been marked A, B, C, and D. The exact positions of the features are listed in table 1.

It is seen that σ for the bulk sample without annealing is similar to that for the disordered film both as regards peak position and intensity. On the other hand, the σ-curves of the ordered film and the annealed bulk sample are observed to be similar. The polished bulk sample without annealing is thus supposed to be essentially disordered, at least within the

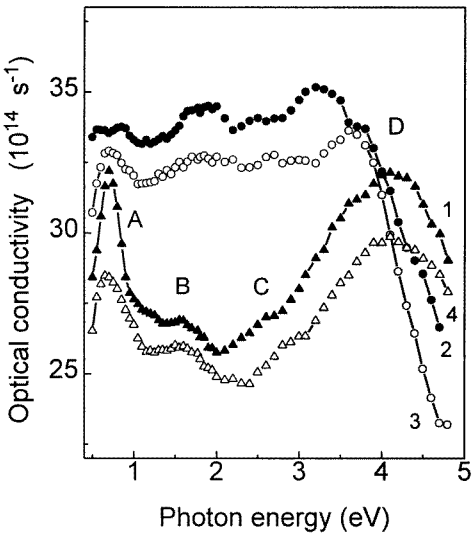

Figure 7. Experimental optical conductivity spectra for ordered (1) and disordered (2) $Fe_{0.52}Al_{0.48}$ films, and for as-polished (3) and annealed (4) bulk FeAl samples. Peaks A–D are discussed in the text.

skin depth. The optical conductivity of the film sample is larger than that of the bulk sample over the whole energy range. This can be attributed to a higher degree of oxidation of the films than of the bulk samples due to the different methods employed for the surface preparation.

Comparison of the spectra of the ordered and disordered FeAl indicates the following trends. The absolute value of σ below 4 eV for the disordered samples is considerably larger than that of the ordered samples. The energy locations of the features change differently in different regions of the spectrum. The peaks A and B of the ordered FeAl are shifted to lower energies, whereas the features C and D shift to higher energies from the respective positions for the disordered alloy. The shifts of the peaks B and C in the visible region are smaller than those of the peak A in the infrared (IR) and peak D in the ultraviolet (UV).

The theoretical optical conductivity for ordered FeAl also has four main features in the photon energy range 0–5 eV (see figure 4). The band-by-band decomposition of σ allows us to determine the initial- and final-energy intervals responsible for these peaks.

There are two narrow manifolds in the DOS curve (see figure 1): the Fe t_{2g} band, which extends from 1 eV below the Fermi level (E_F) to 0.5 eV above the E_F, and the e_g band located from 1 to 2 eV above the E_F. These manifolds are separated by a 'pseudogap' caused by the fact that the nearest neighbours of Fe in the ordered alloy are Al atoms [21]. The peak of σ in the IR region is mostly determined by the interband transitions within the t_{2g} manifold. The features in the visible range arise from the transitions with the final states located in the e_g manifold. In the UV region the most important ones are the transitions with final states also lying near the e_g DOS peak; the initial states are between -4 eV and -3 eV, where Al p and Al s contributions are significant.

In the case in which the crystal lattice is disordered the Fe ions become nearest neighbours with a high probability. As a result the e_g–t_{2g} splitting becomes smaller and the 'pseudogap' vanishes. Thus the contribution from the transitions with the final states in the interval 0.5–1 eV above E_F to the optical spectra grows. As a result the IR maximum

shifts towards higher energies, whereas the UV maximum shifts towards lower energies from their positions for the ordered alloy. In the visible range the peaks become closer.

Thus we explain the experimentally observed variations of the optical properties qualitatively in terms of the influence of disordering on the width of the 'pseudogap'. Since disordering mostly affects the IR and UV parts of the optical spectra, the discrepancies between the theoretical and experimental peak positions in these regions may be attributed to the deviation from $\eta = 1$ in the ordered samples investigated.

4. Conclusions

First-principles calculations of the energy band structures, Fermi surface, and optical properties of FeAl compounds have been performed by the semi-relativistic ELAPW and spin-polarized LMTO methods.

The optical properties of the ordered $Fe_{0.52}Al_{0.48}$ films have been experimentally studied in the 0.5–5.0 eV photon energy range at room temperature, and compared with the results of the first-principles calculations. The origin of the main absorption peaks has been determined. It is shown that large interior parts of the BZ are responsible for the formation of these peaks.

The disordered state of the FeAl alloy films was obtained through the chaos of the gas phase by means of vapour quenching deposition onto substrates cooled by liquid nitrogen. It was experimentally shown that change in the unit-cell symmetry in the order–disorder transition leads to significant changes in the optical properties of the alloys.

The high structural sensitivity of the optical properties of the FeAl alloy can serve as a tool for analysing the perfection of the sample structure, at least in the skin-penetration depth.

Acknowledgments

The authors wish to thank Dr G N Kakazei for performing the TEM study of the FeAl alloy films. This work was supported partially by the Ukrainian Ministry of Science and Technology under project N 2.4/39. This work was also supported by the Korea Research Foundation in Program Year 1996, the Korea Science and Engineering Foundation, and Korea Basic Science Institute.

References

[1] Fleischer R L, Dimidick D M and Lipsitt H A 1989 *Annu. Rev. Mater. Sci.* **19** 231 and references therein
[2] Singh D 1994 *Intermetallic Compounds* vol 1, ed J H Westbrook and R L Fleischer (New York: Wiley)
[3] Müller Ch, Wonn H, Blau W, Ziesche P and Krivitskii V P 1979 *Phys. Status Solidi* b **95** 215
[4] Koenig C and Khan M A 1983 *Phys. Rev.* B **27** 6129
[5] Shavanov F A and Lezhnenko I V 1973 *Fiz. Met. Metalloved.* **35** 1119 and references therein
[6] Hohenberg P and Kohn W 1964 *Phys. Rev.* B **136** 864
[7] Kohn W and Sham L J 1965 *Phys. Rev.* A **140** 1133
[8] Williams V and Barth U 1983 *Theory of the Inhomogeneous Electron Gas* ed S Lundqvist and N H March (London: Plenum)
[9] Krasovskii E E and Schattke W 1995 *Solid State Commun.* **93** 775
[10] Hedin L and Lundqvist B I 1971 *J. Phys. C: Solid State Phys.* **4** 2064
[11] Lehmann G and Taut M 1972 *Phys. Status Solidi* b **54** 469
[12] Blau W, Weisbah J, Merz G and Kleinstück K H 1979 *Phys. Status Solidi* b **93** 713
[13] Kolobova K M and Nemnonov S A 1969 *Fiz. Met. Metalloved.* **27** 1026
[14] Nemoshkalenko V V and Gorskii V V 1969 *Ukr. Phys. J.* **13** 1022

[15] Fischer D W and Baun W L 1967 *J. Appl. Phys.* **38** 229
[16] Kapoor Q S, Watson L M and Fabian D J 1973 *Band Structure Spectroscopy of Metals and Alloys* ed D J Fabian and L M Watson (New York: Academic) p 215
[17] Schwarz K, Neckel A and Nordgren J 1979 *J. Phys. F: Met. Phys.* **9** 2509
[18] Eibler R and Neckel A 1980 *J. Phys. F: Met. Phys.* **11** 1159
[19] Knab D and Koenig C 1990 *J. Phys.: Condens. Matter* **2** 465
[20] Sundararajan V, Sahu B R, Kanhere D G, Panat P V and Das G P 1995 *J. Phys.: Condens. Matter* **7** 6019
[21] Fu C L 1995 *Phys. Rev.* B **52** 3151
[22] Manninen S, Honkimäki V, Hämäläinen K, Laukkanen J, Blaas C, Redinger J, McCarthy J and Suortii P 1996 *Phys. Rev.* B **53** 7714
[23] Okamoto H and Beck P A 1972 *Monatsh. Chem.* **103** 907
[24] Ehrenreich H and Cohen M A 1951 *Phys. Rev.* B **115** 789
[25] Krasovskii E E, Antonov V N and Nemoshkalenko V V 1990 *Phys. Met.* **8** 882
[26] Schlemper K and Thomas L K 1994 *Phys. Rev.* B **50** 17 802
[27] Taylor A and Jones R M 1958 *J. Phys. Chem. Solids* **6** 16
[28] Beattie J R and Conn G M 1955 *Phil. Mag.* **46** 235